CHEMISTRY
A EUROPEAN JOURNAL

DOI: 10.1002/chem.200601372

Porous Iron Oxide Based Nanorods Developed as Delivery Nanocapsules

Ping-Ching Wu,[a] Wen-Shiuan Wang,[b] Ying-Ting Huang,[b] Hwo-Shuenn Sheu,[c] Yi-Wei Lo,[b] Tsung-Lin Tsai,[a] Dar-Bin Shieh,*[d] and Chen-Sheng Yeh*[b]

Abstract: A low-temperature solution approach (90–95 °C) using $FeCl_3$ and urea was carried out to synthesize β-FeOOH nanorods in aqueous solution. The as-synthesized β-FeOOH nanorods were further calcined at 300 °C to form porous nanorods with compositions including both β-FeOOH and α-Fe_2O_3. The derived porous nanorods were engineered to assemble with four layers of polyelectrolytes (polyacrylic acid (PAA)/polyethylenimine(PEI)/PAA/PEI) on their surfaces as polyelectrolyte multilayer nanocapsules. Fluorescein isothiocyanate (FITC) molecules were loaded into the polyelectrolyte multilayer nanocapsules in order to investigate drug release and intracellular delivery in Hela cells. The as-prepared nanocapsules showed ionic strength-dependent control of the permeability of the polyelectrolyte shells. The release behavior of the entrapped FITC from the FITC-loaded nanocapsules exhibited either controlled- or sustained-release trends, depending on the compactness of the polyelectrolyte shells on the nanorod surfaces. Cytotoxicity measurements demonstrate that the native nanorods and the polymer-coated nanorods have excellent biocompatibility in all dosages between 0.1 ng mL^{-1} and 100 μgm L^{-1}. The time dependence of uptake of FITC-loaded nanocapsules by Hela cancer cells observed by laser confocal microscopy indicates that the nanocapsules can readily be taken up by cancer cells in 15 min, a relatively short period of time, while the slow release of the FITC from the initial perimembrane space into the cytoplasm was followed by release into the nucleus after 24 h.

Keywords: cellular uptake · drug delivery · iron · nanorods · polyelectrolytes

Introduction

Functional nanoscale materials have attracted intensive scientific and industrial interest because of their potential applications in optical, electronic, magnetic, and many other fields.[1–3] In the field of inorganic nanomaterials, the carriers used for biomedicine can basically be categorized into two classes of delivery systems. One involves the appropriate surface modification of the nanomaterials (e.g., nanoparticles, nanorods, etc.) to attach desirable biomolecular signals or drugs,[4,5] while the other takes advantage of structural characteristics involving void morphology, such as porosity or hollow interiors, that can be used to serve as nanocontainers, acting as capsulelike carriers and providing protection to limit the accessibility of the biomolecules and drugs to denaturing agents. Targeted delivery of drugs to their desired sites of action and their release in a controlled manner play essential roles in the development of future drug formulations. It is well-known that significant differences in ionic composition exist between extra- and intracellular microenvironments, between normal versus disease tissues, and even in different subcellular compartments which participate

[a] P.-C. Wu, T.-L. Tsai
Institute of Basic Medical Sciences
National Cheng Kung University, Tainan 701 (Taiwan)

[b] W.-S. Wang, Y.-T. Huang, Y.-W. Lo, Prof. C.-S. Yeh
Department of Chemistry and Center for Micro/Nano Science and Technology
National Cheng Kung University, Tainan 701
Taiwan National Cheng Kung University (Taiwan)
E-mail: csyeh@mail.ncku.edu.tw

[c] Dr. H.-S. Sheu
National Synchrotron Radiation Research Center
Hsinchu 30076 (Taiwan)

[d] Prof. D.-B. Shieh
Institute of Oral Medicine and Department of Stomatology and Center for Micro/Nano Science and Technology
National Cheng Kung University, Tainan 701 (Taiwan)
Fax: (+886)-6-274-0552
E-mail: dshieh@mail.ncku.edu.tw

Supporting information for this article is available on the WWW under http://www.chemeurj.org/ or from the author. This information contains HRTEM and SAED patterns of the β-FeOOH nanorods, FTIR spectra of the β-FeOOH and pure urea, SAED image of a single nanorod after calcination, ζ potential and HRTEM analysis of the polyelectrolyte multilayer nanocapsules, and nitrogen adsorption–desorption isotherm measurements.

in various cellular functions.[6] Cells maintain higher concentrations of potassium ion, while sodium and chloride ions are major species in the extracellular fluid. Active ion transporters on the membrane permit high proton concentrations in the lysosome of the cell. Thus, in practice, capsulelike nanocarriers with appropriate engineering in the form of chemical modification of their pore gates could serve as ideal platforms for controlled drug release in response to the microenvironment of the surrounding tissue or even subcellular space. To date, however, the use of inorganic nanomaterials as nanocontainers for delivery purposes has been limited and has mainly been focused on silica-based materials, such as silica nanotubes,[7,8] mesoporous silica nanoparticles, and nanorods.[9–11] Unfortunately, although some of the results have demonstrated drug release capability,[7–9] no comprehensive elucidation of the stimuli-responsive release of drugs by those delivery systems has yet been addressed in detail, so there remains a need for more detailed studies for further applications in cells or tumors. Lin et al. have demonstrated a strategy of controlling the permeabilities of mesoporous nanospheres[10] and nanorods[11] by capping the entry ports of the mesopores with nanoparticles (for example, quantum dots (CdS) and supermagnetic iron oxides (Fe_3O_4)) in which both nanoparticles and pore surfaces were functionalized and covalently linked by a disulfide bond. The release of drugs from inside the pores can be triggered by the cleavage of disulfide bonds by disulfide reducing agents.

Here we have developed porous iron oxide based nanorods coated with polyelectrolyte polymers, forming nanocapsules. The permeabilities of the as-synthesized nanocapsules are modified by ionic strength and show either stimuli-responsive controlled behavior or sustained-release behavior, depending on the compactness of the polyelectrolyte shells on the nanorod surfaces.

For the synthesis of one-dimensional β-FeOOH nanocrystals, it is known that the hydrolysis of acid $FeCl_3$ results in spindle-shaped structures.[12] Recently, β-FeOOH nanorods have been fabricated by the hydrothermal method, either with use of $FeCl_3$ and cetyltrimethylammonium bromide as starting materials (Zhang et al.[13]), or in water or water/ethanol cosolvent systems containing $FeCl_3$ and $NaNO_3$ as precursors (Qian et al.[14]). In this work, β-FeOOH nanorods were synthesized by a low-temperature solution approach (90–95 °C), starting with $FeCl_3$ as a precursor in the presence of urea in an aqueous solution, the urea serving as a source of hydroxide ions during the hydrolysis of iron salts to form iron oxyhydroxides (FeOOH). The as-synthesized β-FeOOH nanorods were then calcined in the forms of porous structures with compositions including both β-FeOOH and α-Fe_2O_3 (β-FeOOH/α-Fe_2O_3) for study of their drug release kinetics and intracellular delivery properties in the Hela cancer cell line. The formation of porous nanorods was the result of partial decomposition of β-FeOOH, creating voids and giving rise to incomplete phase transition for products containing both β-FeOOH and α-Fe_2O_3.

As a porous structure is employed to act as a carrier, an appropriate shield to cover the pore orifice is required in order to encapsulate and protect the drugs before they are safely delivered to the target. Permeability is a concern for release of substances from a container's interior in a controlled way at the desired target. Polyelectrolyte materials have a variety of biomedical applications: polyelectrolyte fibrous structures can serve, for example, as scaffolds for tissue engineering.[15] In addition, polyelectrolyte microcapsules have demonstrated potential for host–guest encapsulation and controlled release of encapsulated materials from their interiors.[16–19] The polyelectrolyte capsules are regarded as representative candidates for stimuli-responsive nanocontainers because the conformations of polyelectrolytes are sensitive to changes in pH, salt, heat, and light stimuli. PEI (polyethylenimine) has been recognized as an efficient delivery vehicle for intracellular delivery, accessing cells through endocytosis.[20–22] Here a layer-by-layer (LbL) method based on electrostatic attraction between oppositely charged polymer layers was utilized to assemble first a negatively charged polyacrylic acid (PAA) layer, followed by a positively charged PEI layer in a sequential fashion on the porous nanorod (β-FeOOH/α-Fe_2O_3) surface, with PEI as an outermost layer in the polyelectrolyte shells. So far, such polyelectrolyte-based capsules have mainly been used in the fabrication of spherelike structures, while the development and application of polyelectrolyte rodlike capsules as biomolecular carriers is still very rare. The as-prepared biocompatible iron oxide based nanorod deposition of polyelectrolyte layers (PAA/PEI/PAA/PEI) is selectively swollen by salt (ionic strength), which triggers the release of encapsulated materials from the interiors. The release behavior is also found to be strongly affected by the compactness of the polyelectrolyte shells on the nanorod surfaces. Furthermore, laser confocal microscopy was conducted to investigate the time dependence of the subcellular distribution of the nanocapsules in Hela cancer cells.

Results and Discussion

Synthesis of β-FeOOH nanorods was achieved by addition of urea to an aqueous solution of $FeCl_3{\cdot}6H_2O$ in a reflux process at temperatures of 90–95 °C over 12 h. Figure 1a shows a typical TEM image of the as-synthesized FeOOH products and reveals FeOOH formed into rodlike structures with diameters of 38 ± 5 nm and lengths of 480 ± 45 nm. An X-ray diffraction (XRD) pattern of the as-synthesized FeOOH nanorods is shown in Figure 1b. All the deflection peaks can be indexed to a tetragonal β-FeOOH phase, consistent with the reported values (JCPDS No. 34–1266). The high-resolution transmission electron image (HR-TEM) and the corresponding selected area electron diffraction (SAED) patterns show that the fringe spacing of 0.22 nm is consistent with the (301) and (01) lattice planes, while the 0.15 nm spacing corresponds to the (002) planes (Supporting Information). Combined with the SAED result, the crystal-

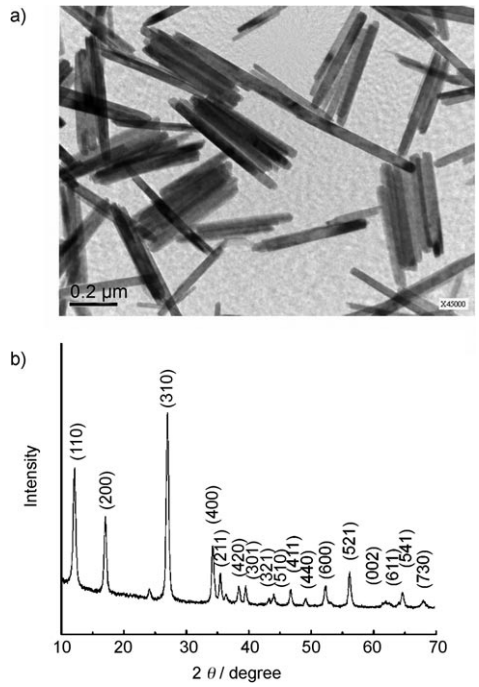

Figure 1. a) TEM image of the β-FeOOH nanorods. b) X-ray diffraction pattern showing β-FeOOH structure.

line orientation of the β-FeOOH nanorod is along [200] for the long axis and the derived β-FeOOH nanorods are single crystals with a tetragonal crystal structure. In this synthesis, $FeCl_3$ was used in the presence of urea, which provides hydroxide ions during the hydrolysis of iron salts, to prepare β-FeOOH. IR measurements were performed and it was found that the FeOOH surface had adsorbed urea molecules (Supporting Information).

Since the ultimate purpose was the creation of porosity in nanorods, a simple calcination process was used to obtain porous structures, it being known that FeOOH can be converted into α-Fe_2O_3 at around 500 °C.[13,14] The nanorod formation was monitored as a function of calcination temperature. Figure 2 shows typical SEM images of the resulting products, and their morphologies at different temperatures were observed. As can be seen in Figure 2a, the nanorods had retained their shapes, without apparent void creation on their surfaces, after calcination at 200 °C for 1 h. After heating at 300 °C, the morphology clearly still appeared as that of a porous structure and each nanorod still remained intact (Figure 2b); Figure 2c shows a single porous nanorod, in which the pores have been created in irregular shapes. If, however, the temperature was further increased up to 400 °C, the nanorods started to fuse together and the morphology of their edges became rugged, as can be seen in Figure 2d. Apparently, the selection of the calcination temperature is crucial in the preparation of porous nanorods, and in this case calcination at 300 °C is the best choice for producing porous rods without serious structural collapse. As mentioned earlier, complete conversion of FeOOH into α-Fe_2O_3 requires a heating temperature of up to 500 °C. The nanorods obtained at 300 °C might represent incomplete phase transformation and thus have mixed compositions. High-resolution XRD images with a synchrotron X-ray source ($\lambda =$ 0.9537 Å) were taken to characterize the derived nanorods. Figure 3 clearly indicates that the diffraction patterns include both β-FeOOH and α-Fe_2O_3 reflections and that the porous nanorods are composed of β-FeOOH and α-Fe_2O_3 structures due to incomplete phase transformation. SAED

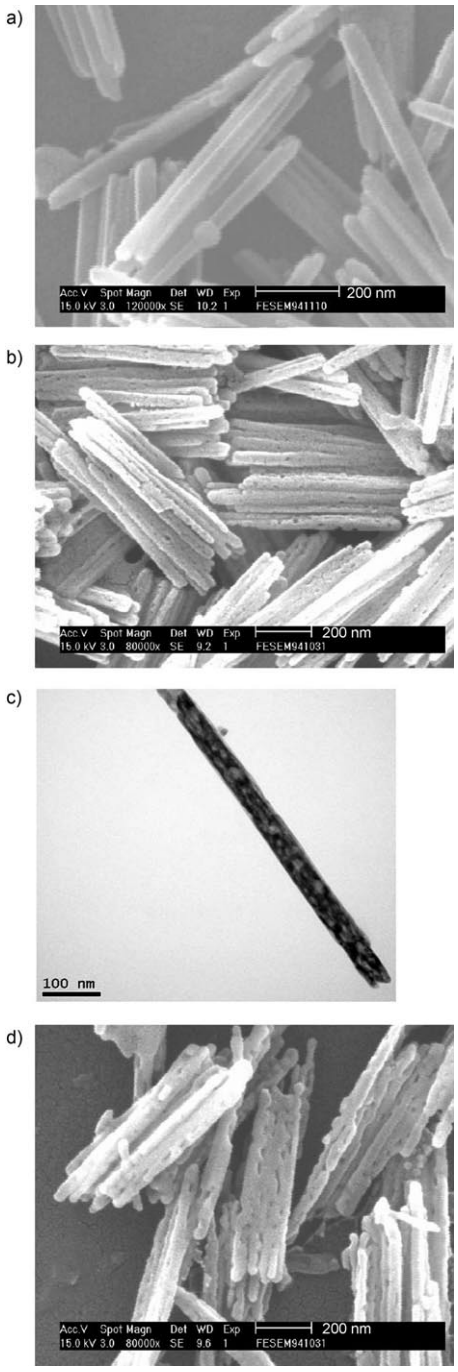

Figure 2. SEM images of the porous nanorods at different temperatures: a) 200 °C, b) 300 °C, and d) 400 °C, together with c) TEM image of a single porous nanorod at 300 °C.

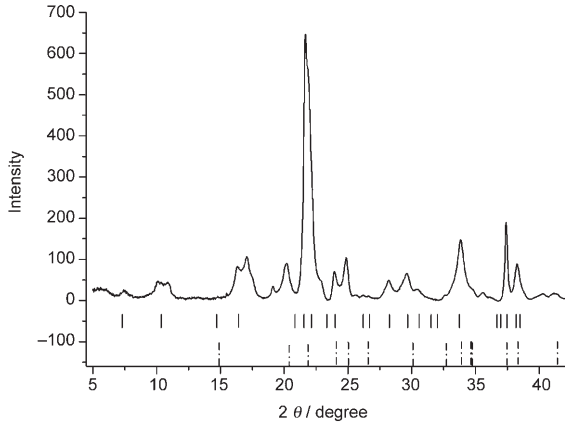

Figure 3. X-ray powder diffraction patterns for the porous nanorods measured by high-resolution XRD with a synchrotron X-ray source ($\lambda =$ 0.9537 Å). The solid and dash–dot line marks represent β-FeOOH and α-Fe_2O_3, respectively.

measurements were also conducted with a single porous nanorod, and both β-FeOOH and α-Fe_2O_3 compositions contained in one nanorod were characterized (Supporting Information). The pore size distribution of the porous β-FeOOH/α-Fe_2O_3 nanorod was measured by the nitrogen adsorption–desorption isotherm and Barrett–Joyner–Halenda (BJH) methods. The isotherm characterized the β-FeOOH/α-Fe_2O_3 nanorods as having a mesoporosity of type IV with a distinct hysteresis loop in the range of 0.4–1.0 P/P_o, indicating H2-type hysteresis (Supporting Information). This H2-type hysteresis represents a disordered and inhomogeneous distribution of pore sizes in the presence of an interconnected network of pores. The resulting porous nanorods showed a BET surface area of 45.96 $m^2 g^{-1}$ with a pore size distribution of 2–20 nm.

The derived porous nanorods were further engineered to assemble with multilayer polyelectrolytes on their surfaces as carriers. The successive deposition of the multilayer shells on the nanorods was monitored by measuring the ζ potential changes of the rods after each deposition (Supporting Information). Native porous nanorods have a ζ potential of approximately 22.58 mV. After deposition of the first layer, the negative PAA caused a reversal in ζ potential to approximately −41.63 mV, while the subsequent deposition of the PEI produced an inversion to approximately 42.21 mV. The layer-by-layer method was applied to form multilayer films on the particle surface through the electrostatic attraction between oppositely charged species, and alternating ζ potential values were observed between positive PEI and negative PAA. High-resolution TEM (HRTEM) showed that the resulting multilayer polyelectrolyte shells had thicknesses of 4–5 nm (Supporting Information).

Fluorescein isothiocyanate (FITC) was applied to investigate the release kinetics of the polymer-coated porous nanorods. In this case, FITC was loaded into porous nanorods, and this was followed by the deposition of the four-layer polyelectrolyte (PAA/PEI/PAA/PEI). It was found that ≈94% of the FITC molecules could be loaded into the porous nanorods. Although the formation of the cavities in the nanorods had been specifically designed to entrap targeted molecules, FITC adsorption on the walls might nonetheless have occurred at the same time. For the preparation of FITC-loaded nanorods, an aqueous solution containing porous nanorods (1 mL) was incubated with FITC (0.1 mM, 100 μL), producing a pH ≈5 solution. FITC is a proteolytic acid with three pK_a values of 2.2, 4.4, and 6.7, and it has been reported that FITC exists as neutral and monoanion species between pH 2.8 and 5.5.[23] Interaction between the COO^- groups of the FITC molecules and the positive surfaces of the rods could possibly have resulted in the adsorption of FITC on the walls. Figure 4a demonstrates the release profile of FITC from polyelectrolyte-coated nanorods made with a deposition time (the incubation time for polyelectrolyte deposition onto the porous nanorods) of 2 h for each layer before coating of the subsequent layer. In distilled water, over a pH range of 4 to 9, most of the FITC molecules were still locked inside the porous nanorods even after 48 h of incubation, while a PBS (pH 7) environment had triggered a sixfold release of the fluorochrome into the

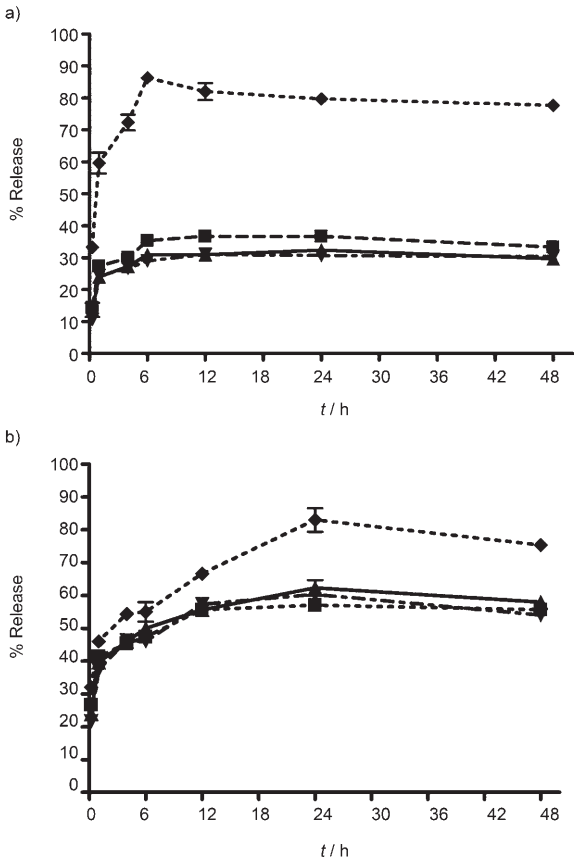

Figure 4. In vitro release studies of: a) densely packed (2 h adsorption for each polyelectrolyte layer) FITC-loaded nanorods performed in distilled H_2O versus phosphate buffered saline (pH 7), and b) loosely packed (30 min adsorption for each polyelectrolyte layer) FITC-loaded nanorods performed in distilled H_2O versus phosphate buffered saline (pH 7). ◆ PBS, ■ pH 4 ddH_2O, ▲ pH 7 ddH_2O, ▼ pH 9 ddH_2O (dd = doubly distilled).

supernatant in as little as 6 h. The environment-sensitive release of FITC indicates controlled-release behavior triggered by the presence of PBS. Apparently, the presence of ionic species had strongly affected the permeabilities and the release performances of the as-prepared polyelectrolyte-coated nanorods.

In addition, an experiment parameter was varied by changing the deposition times of each layer onto the nanorod surfaces, with the incubation times between polyelectrolytes and porous nanorods in the course of preparation of the polyelectrolyte shells being shortened from 2 h to 30 min. Once again, pH-independent release of FITC enhanced by the presence of PBS was observed (Figure 4b). The release profile of FITC gradually increased over time and reached a plateau at 24 h, implying sustained-release behavior. From the results shown in Figure 4a,b, the use of different deposition periods for coating of the polyelectrolytes onto the nanorod surfaces resulted in distinct release behavior in the as-prepared nanocapsules, which might be associated with the compactness of the polyelectrolyte deposition on the nanorod surfaces. That is, use of a 2 h adsorption period for each polyelectrolyte layer yielded densely packed nanocapsules while a 30 min deposition for each layer resulted in loosely packed shells. While detailed reasons for the distinct difference in release behavior between densely and loosely packed nanocapsules are yet to be confirmed, it is possible that in the case of the densely packed nanocapsules, the polyelectrolytes could have diffused into the pores of nanorods, occupying and blocking the spaces and pathways to prevent the release of the entrapped FITC in distilled water. The counterions (in PBS) that enter into the polyelectrolyte layers, however, may cause expansion of the shells, which in turn could encourage the release of the entrapped molecules, which might then readily penetrate the capsule walls. In the case of short-period polyelectrolyte deposition, on the other hand, the loosely packed polymer shells have limited stereoconfinement properties to lock the encapsulated chemicals, so sustained-release behavior is observed rather than a salt-dependent burst release, as seen in the densely packed nanocapsules. It is worth mentioning that we have collected nanocapsules to inspect their polyelectrolyte shells after incubation at various pH values (4, 7, and 9) and salt (PBS) concentrations. HRTEM images showed that all polymer coatings remained on the nanorod surfaces (Supporting Information), which suggests that the release behavior is not the result of the polymers being stripped off.

We have shown that the as-prepared nanocapsules potentially exhibit salt-induced permeability changes in their polyelectrolyte shells. Further studies of variation of the salt (NaCl) concentration are shown in Figure 5. Densely packed nanocapsules (2 h deposition for each polymer layer) were used, with controlled-release profiles for the ionic strength studies. As can be seen in Figure 4a, the release quantity reaches a maximum level at 6 h. Throughout this series of measurements, FITC release was measured at the 6 h timepoint and the pH level was kept constant at 7. Figure 5 shows the occurrence of a concentration-dependent FITC release, increasing from 0.001 to 1 M, which demonstrates that the as-prepared nanocapsules are sensitive to ionic strength. The changes in the permeabilities of the polyelectrolytes upon variation in the ionic strength are sufficient to loosen the polyelectrolyte shells, thus enabling the release of the encapsulated FITC from their interiors.

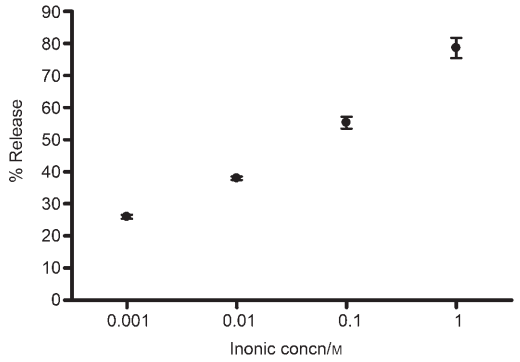

Figure 5. In vitro release studies of densely packed (2 h adsorption for each polyelectrolyte layer) FITC-loaded nanocapsules monitored as a function of NaCl concentration at a pH of 7. The release quantities were determined at the 6 h timepoint for each NaCl concentration.

Since the polyelectrolyte-coated nanorods had shown potential as drug delivery nanocapsules in biomedical applications, cell viability experiments were conducted to evaluate the cytotoxicity of the as-prepared nanorods (Figure 6). Here, loosely packed nanocapsules (30 min deposition for each polymer layer) were selected as an example in order to study their cytotoxicities. The WST-1 assay shows that both the as-prepared native nanorods and the polymer-coated

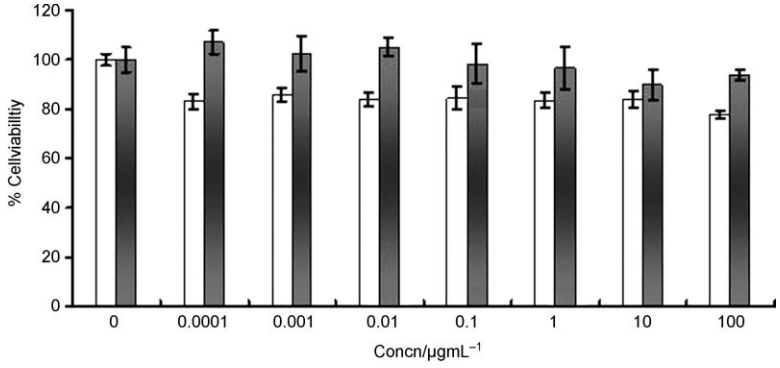

Figure 6. The biocompatibilities of the nanorods with (black columns) or without (white columns) polymer coatings were analyzed by WST-1 assay.

nanorods gave satisfactory results for in vitro biocompatibility in all dosages between 0.1 ng mL^{-1} and 100 μgm L^{-1}.

Finally, the loosely packed nanocapsules (30 min deposition for each polymer layer) were used for laser confocal microscopy to evaluate time-dependent intracellular release of FITC from the nanocapsules in Hela cancer cells. As shown in Figure 7a, the intracellular fluorescent signal started to be detectable 15 min after incubation of the Hela cells with FITC-loaded nanocapsules, displaying as a diffuse weak fluorescent. In the differential interference contrast (DIC) mode, only a few black spots corresponding to the presence of nanorod aggregates were observed. Both DIC and FITC channels (representing fluorescence images) showed time-dependent accumulation of FITC and the FITC-loaded nanocapsules in the Hela cells. Figure 7b shows the quantified accumulation of FITC fluorescent signals from the FITC image as measured with the use of Alpha Image 2200 software. Five different areas of the green fluorescent expression in each cell were selected and calculated by deduction of the background. The data displayed trends similar to those outlined in Figure 4b, in which the release of FITC increased over time. The reconstructed saggital sections of the cancer cells in the area across the red line are shown in the bottom two rows of Figure 7a. As shown in the reconstructed saggital sections of the combined FITC and DAPI (nuclear stain in blue color) channels, the released FITC had started to diffuse from the cytoplasm into the nucleus in as little as 1 h after exposure, although most of the FITC signal still remained in the cytoplasm. At 24 h, a significant increase in the intensity of FITC could be detected in both nucleus and cytoplasm. The saggital sections of representative cancer cells showed that FITC initially accumulated close to the peri-membrane space, followed by the cytoplasm, then the nucleus. As the FITC-loaded nanorods presented no fluorescent signals in the fluorescent spectroscopy analysis, the observed fluorescent signal should come from the released chemicals from the rods. Phagosome activation upon uptake of foreign materials, for example nanomaterials, could have provoked the influx of an enormous concentration of ROS (ROS = reactive oxygen species) into the endocytic vesicle, resulting in an accumulation of anionic charge which was compensated for by an influx surge of K^+ ions across the membrane in a pH-dependent manner.[24,25] Therefore, a microenvironment of relatively high salt concentration, which might further encourage local release of FITC from the as- synthesized nanorods, was created, as demonstrated in the releasing kinetic studies. Overall, the above studies, including release kinetics, cytotoxicity, and cellular uptake and intracellular drug delivery, indicate that biocompatible porous iron oxide nanorods with great potential for biomedical applications both as functional carriers and as imaging agents have been developed.

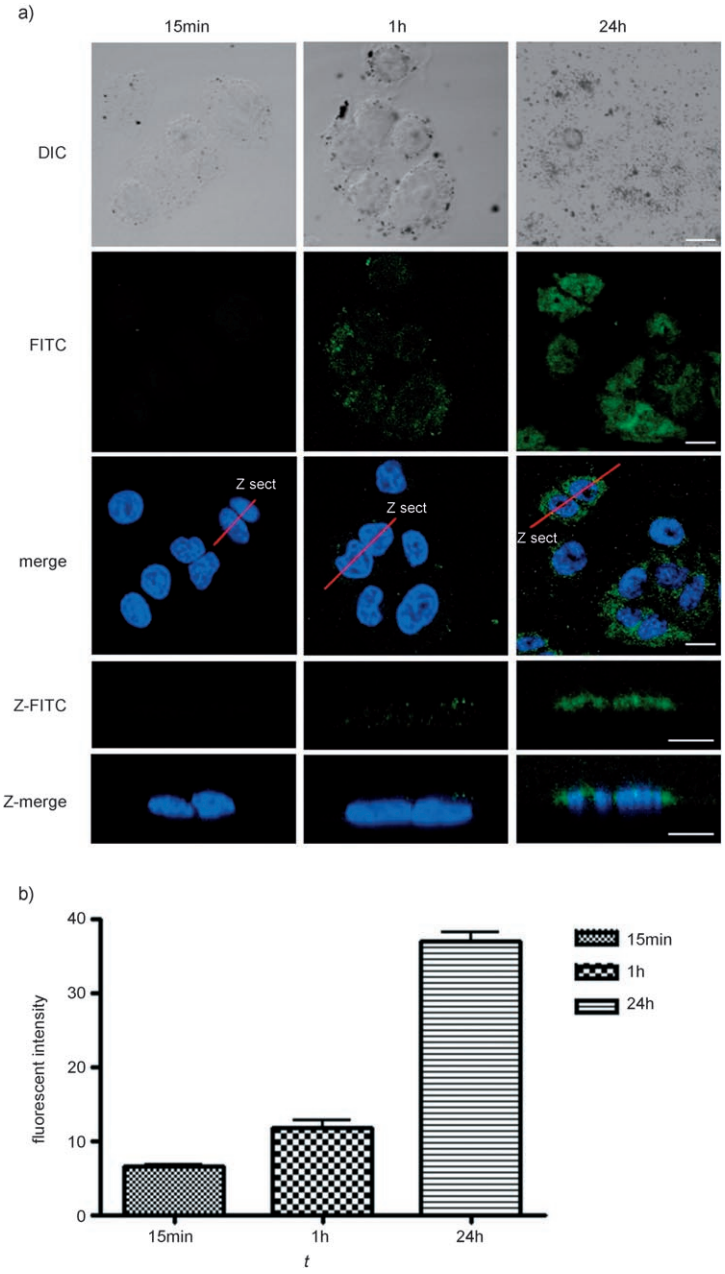

Figure 7. Laser confocal microscopy of Hela cells exposed to FITC-loaded porous iron oxide nanorods for 15 min, 1 h, and 24 h. a) Aggregations of nanorods presented as dark spots could be observed by DIC microscopy observation. The FITC images showing accumulation of FITC fluorescence signal in the Hela cells were observed in a time-dependent manner. The merged images show the location of nuclei (blue color) and FITC (green color). The reconstructed saggital sections of the cancer cells in the area across the red lines are shown in the bottom two rows. Time-dependent accumulation of FITC was observed (Z-FITC). The Z-merge showed that FITC also diffuses through the nucleus (scale bar: 10 μm). b) The FITC image of quantified accumulation of the FITC fluorescent signal.

Conclusions

Porous iron oxide based nanorods which can readily be capped with multilayer polyelectrolytes in order to serve as

nanocapsules have been demonstrated. These nanocapsules displayed ionic strength-triggered permeability changes in their polyelectrolyte shells and can be used either as stimuli-responsive controlled or as sustained-release delivery carriers. Furthermore, the amine groups on the shells (PEI polymer) of the nanocapsules, which can provide further surface modification for attachment of targeting moieties and subcellular delivery signals, coupled with the excellent in vitro biocompatibility and the efficient controlled release of drugs, all suggest great potential for use in multifunctional composite capsules for drug delivery to specific targets.

Experimental Section

Chemicals: All chemicals used in this work were analytical grade reagents obtained from commercial sources without further purification. The chemical reagents were ferric chloride ($FeCl_3{\cdot}6H_2O$; J. T. Baker), urea ($(NH_2)_2CO$; Showa), polyacrylic acid (PAA, Mw: 2000; Aldrich), polyethyleneimine (PEI, Mw: 25000; Aldrich), and fluorescein isothiocyanate (FITC; Sigma).

Preparation of porous iron oxide based nanorods: To synthesize β-FeOOH nanorods, the following method was used. $FeCl_3{\cdot}6H_2O$ (1.0134 g) and $(NH_2)_2CO$ (0.60 g) were dissolved in distilled water (10 mL) with constant stirring over 10 min. The solution was then transferred to a flask and maintained at 90–95 °C under a reflux condenser for a period of 12 h, resulting in the formation of a yellow precipitate. This precipitate was collected and rinsed repeatedly with distilled water to provide β-FeOOH nanorods. The resulting β-FeOOH nanorods were then calcined at 300 °C for 1 h to form porous nanorods with compositions including both β-FeOOH and α-Fe_2O_3.

Sequential deposition of polyelectrolytes onto porous nanorod surfaces with loading of FITC: The porous β-FeOOH/α-Fe_2O_3 nanorods with native surfaces were incubated with FITC (0.1 mM, 100 μL) in an aqueous solution (1 mL) and the system was stirred for 30 min. This was followed by the addition of negatively charged PAA (10 mM, 100 μL) for an additional incubation period (30 min or 2 h). The PAA-coated nanocapsules were collected by centrifugation (13000 rpm, 10 min), followed by washing with distilled water to remove residual FITC and PAA, and were then re-dispersed in H_2O (1 mL), with PEI (1 mM, 100 μL) added for incubation (30 min or 2 h). Once again, the excess PEI was removed by centrifugation for 10 min at 13000 rpm to provide PAA/PEI-coated nanorods. Through a recursive operation, porous nanorods were encapsulated into polyelectrolyte shells with two PAA/PEI layer pairs (PAA/PEI/PAA/PEI).

Release studies on the polyelectrolyte multilayer nanocapsules: To evaluate the effects of pH and a physiological buffer on the release kinetics of FITC from the porous nanorods, distilled water (1 mL) at pH values of 4, 7, and 9 and phosphate-buffered saline (PBS) were added to the dried FITC-loaded nanocapsules for incubation for different time periods of 20 min and 1, 4, 6, 12, 24, and 48 h. Subsequently, the supernatants from the solutions were collected by centrifugation for 10 min at 15000 rpm and subjected to fluorescent signal quantification of FITC with a fluorescence spectrophotometer (F-2500, Hitachi, Japan).

The effect of salt (NaCl) concentration on FITC release from the polyelectrolyte multilayer nanocapsules: A series of NaCl concentrations (0.001, 0.01, 0.1, and 1 M) in distilled water were prepared and mixed with the FITC-loaded nanocapsules. For the FITC-loaded nanocapsules, each layer of the polymer had received 2 h of incubation time with the nanorods to form polyelectrolyte shells. The FITC release characteristics of the FITC-loaded nanocapsules were evaluated by measurement of the fluorescence intensities of the supernatants.

Preparation of cell lines: Human cervical carcinoma cell line Hela cells and African green monkey kidney cell line Vero cells were obtained from the American Type Culture Collection (ATCC, Manassas, VA) and maintained in a minimum essential medium containing fetal bovine serum (10%) and penicillin (1%), L-glutamine (2 mM), nonessential amino acid (0.1 mM), and Na pyruvate (1 mM, Gibco, Labs, Life. Technologies, NY). The cells were incubated in 37 °C humidified air/CO_2 (5%). For further experiments, cells were harvested by short exposure to trypsin/EDTA (Gibco, Labs, Life. Technologies, NY), and seeded at densities of 2×10^5 and 5×10^3 cells per well in a six-well and a 96-well tissue culture plate, respectively.

Biocompatibility evaluation: The biocompatibility of the as-synthesized nanorods in the Vero cell line was evaluated by a WST-1 assay (Roche Diagnostics, Mannheim, Germany). Briefly, 5×10^3 cells per well were seeded in a 96-well culture plate and incubated overnight. Different concentrations of the nanorods with or without polyelectrolyte coatings were added to the medium (0.1 ng–100 μg), which was then used to replace the original culture medium, and incubation was continued for an additional 24 h. The culture medium was removed and replaced with the new culture medium (100 mL) containing WST-1 reagent (10%). The cells were then incubated for 1.5 h to allow formation of the formazan dye at 37 °C. The reaction product (100 mL) was transferred to a new ELISA plate and the A_{450} was measured with a Sunrise ELISA plate reader (Tecan Austria Gesellschaft mbH., Salzburg, Austria). The cell growth activity as a percentage of the untreated control was then calculated.

Laser confocal microscopy of the FITC-loaded nanocapsules exposed to Hela Cells: Hela cells (American Type Culture Collection, VA) were conditioned to culture in a CO_2-independent medium (Invitrogen, CA) in 4-well chamber slides (Nalge Nunc International, NY) with an initial seeding density of 10^6 cells per well, and incubated overnight before further experiments. A final concentration of 100 μM FITC-loaded nanocapsules was incubated with the cultured cells for 15 min, 1 h, and 24 h, and then washed twice with culture medium. The cells were then fixed with paraformaldehyde (4%) and mounted with Vectashield media (Vector Laboratories, Burlingame, CA) for laser confocal microscopy observation (OLYMPUS FV1000 Confocal Microscope, Olympus, Japan).

Characterization: The crystalline structures were identified by thin-film X-ray diffraction (XRD) with a Rigku 18 kW RINT 2000 X-ray diffractomer with the use of $Cu_{K\alpha}$ radiation ($\lambda = 1.54060$ Å). The synchrotron X-ray powder diffraction data for structure analysis were obtained by use of the wiggler beamline BL01C2 of the National Synchrotron Radiation Research Center (NSRRC), Taiwan. The X-ray wavelength was 0.9537 Å, delivered with a double crystal monochromator with two Si(111) crystals. Electron micrographs from transmission electron microscopes (JEOL 3010, at 300 KV and PHILIPS CM-200, at 200 KV) were obtained by placing a drop of the sample on a copper mesh coated with an amorphous carbon film, followed by evaporation of the solvent in a vacuum desiccator. Scanning electron microscopy (SEM) images of the as-synthesized products on the copper substrates were obtained with a Philips XL-40FEG field emission scanning electron microscope. The ζ potential was measured by use of a Zetasizer analyzer (Malvern, UK). IR spectra were measured on a JASCO 200E Fourier Transformation Infrared Spectrometer. N_2 adsorption measurements were performed at 77 K, with a Micromeritics ASAP 2010 system with use of Brunauer–Emmett–Teller (BET) calculations for the surface area and Barret–Joyner–Halenda (BJH) calculations for pore size distribution from the desorption branch of the isotherm.

Acknowledgement

We thank the National Science Council of Taiwan for financially supporting this work.

[1] A. P. Alivisatos, *Science* **1996**, *271*, 933.
[2] J. Hu, T. W. Odom, C. M. Lieber, *Acc. Chem. Res.* **1999**, *32*, 435.
[3] X. Duan, Y. Huang, Y. Cui, J. Wang, C. M. Lieber, *Science* **1998**, *279*, 208.
[4] G. Ozin, *Adv. Mater.* **1992**, *4*, 612.

[5] V. R. Rámila, A. P. P. del Real, J. Pérez-Pariente, *Chem. Mater.* **2001**, *13*, 308.
[6] K. D. Collins, *Biophys Chem.* **2006**, *119*, 271.
[7] S. J. Son, J. Reichel, B. He, M. Schuchman, S. B. Lee, *J. Am. Chem. Soc.* **2005**, *127*, 7316.
[8] C. C. Chen, Y. C. Liu, C. H. Wu, C. C. Yeh, M. T. Su, Y. C. Wu, *Adv. Mater.* **2005**, *17*, 404.
[9] J. Kim, J. E. Lee, J. Lee, J. H. Yu, B. C. Kim, K. An, Y. Hwang, C. H. Shin, J. G. Park, J. Kim, T. Hyeon, *J. Am. Chem. Soc.* **2006**, *128*, 688.
[10] C. Y. Lai, B. G. Trewyn, D. M. Jeftinija, K. Jeftinija, S. Xu, S. Jeftinija, V. S. Y. Lin, *J. Am. Chem. Soc.* **2003**, *125*, 4451.
[11] S. Giri, B. G. Trewyn, M. P. Stellmaker, V. S. Y. Lin, *Angew. Chem.***2005**, *117*, 5166; Angew. Chem. Int. Ed. **2005**, 44, 5038.
[12] R. M. Cornell, U. Schwertmann, *The Iron Oxides*, VCH, Weinheim, Germany, **1996**, p. 71.
[13] X. Wang, X. Chen, L. Gao, H. Zheng, M. Ji, C. Tang, T. Shen, Z. J. Zhang, *Mater. Chem.* **2004**, *14*, 905.
[14] H. F. Shao, X. F. Qian, J. Yin, Z. K. Zhu, *J. Solid State Chem.* **2005**, *178*, 3130.
[15] A. C. A. Wan, B. C. U. Tai, J. K. Leck, Y. Ying, *Adv. Mater.* **2006**, *18*, 641.
[16] M. Sauer, W. Meier, *Chem. Commun.* **2001**, 55.
[17] M. Sauer, D. Streich, W. Meier, *Adv. Mater.* **2001**, *13*, 1649.
[18] G. B. Sukhorukov, A. A. Antipov, A. Voigt, E. Donath, H. Möhwald, *Macromol. Rapid Commun.* **2001**, *22*, 44.
[19] C. S. Peyratout, L. Dähne, *Angew. Chem.* **2004**, *116*, 3850; *Angew. Chem. Int. Ed.* **2004**, *43*, 3762.
[20] W. T. Godbey, K. K. Wu, A. G. Mikos, *J. Control. Release* **1999**, *60*, 149.
[21] W. T. Godbey, K. K. Wu, A. G. Mikos, *Proc. Natl. Acad. Sci. USA* **1999**, *96*, 5177.
[22] M. Lecocq, S. Wattiaux-DeConink, N. Laurent, R. Wattiaux, M. Jadot, *Biochem. Biophys. Res. Commun.* **2000**, *278*, 414.
[23] M.-R. S. Fuh, L. W. Burgess, T. Hirschfeld, G. D. Christian, F. Wang, *Analyst* **1987**, *112*, 1159.
[24] A. B. Stefaniak, R. A. Guilmette, G. A. Day, M. D. Hoover, P. N. Breysse, R. C. Scripsick, *Toxicol. in Vitro* **2005**, *19*, 123.
[25] E. P. Reeves, H. Lu, H. L. Jacobs, C. G. Messina, S. Bolsover, G. Gabella, E. O. Potma, A. Warley, J. Roes, A. W. Segal, *Nature* **2002**, *416*, 291.

Received: September 25, 2006
Published online: February 15, 2007

